DOI: 10.13009/EUCASS2023-376
Aerospace Europe Conference 2023 – 10TH EUCASS – 9TH CEAS

Nonlinear Dynamic Inversion Autopilot Design for Aerial Vehicles with Thrust Vector and Aerodynamic Control

Rabiya BIYIKLI†, Raziye TEKIN**, and İlkay YAVRUCUK****
* Roketsan Inc., ** Roketsan Inc., ***Technical University of Munich*
PK.30 Elmadağ, Ankara, Turkey, 80333 Munich, Germany
rabiyabiyikli@gmail.com – razytekin@gmail.com – yavrucuk@gmail.com
† Corresponding Author

Abstract
This study suggests a Nonlinear Dynamic Inversion (NDI) autopilot for roll angle, lateral and longitudinal acceleration control of an aerial vehicle with both thrust vector and aerodynamic control. Sensitivity analysis of the autopilot under uncertainties, performance comparison with a linear autopilot, and a guided scenario with realistic measurement models are examined. The study uses two-loop cascaded structure with second-order reference models and proportional-integral controllers in each control channel. In addition, output redefinition is practiced to solve the non-minimum phase problem with NDI acceleration autopilots related to aerodynamic tail-controlled missile that is considered in the study.

Nomenclature

ϕ, θ, ψ = Euler angles (roll, pitch, yaw)
$F_B^{(b)}$ = Force on the body
$M_B^{(b)}$ = $[L \quad M \quad N]^T$ Moment on the body
u, v, w = Translational velocity on body axis
ω = $[p \quad q \quad r]^T$ Angular velocity on body axis
S_{ref}, l_{ref} = Reference area, reference length
m = Mass
I = Inertia
Q = Dynamic pressure
T = Thrust
θ_T, ψ_T = Deflection of thrust from centerline in pitch and yaw
$\vec{g}$ = Local gravity vector
$\vec{l}$ = Jet vanes moment arm
L_{BE} = Transformation matrix from earth fixed frame to body frame
$\omega_{cas}, \zeta_{cas}$ = Natural frequency, damping ratio of actuators
ω_{rm}, ζ_{rm} = Natural frequency, damping ratio of reference model
v_i, v_o = Inner loop virtual control inputs, inner loop virtual control inputs
A_i = Decoupling matrix of inner loop from input
A_o = Decoupling matrix of outer loop from body rates
b_i = Nonlinear dynamics of inputs to body rates
b_o = Nonlinear dynamics of body rates to outputs
y = Outputs
δ_A = $[\delta_{A_e} \quad \delta_{A_r} \quad \delta_{A_a}]^T$ Effective aerodynamic control inputs (Elevator, Rudder, Aileron)
δ_T = $[\delta_{T_e} \quad \delta_{T_r} \quad \delta_{T_a}]^T$ Effective Thrust jet vane control inputs (Elevator, Rudder, Aileron)
K_ω = Inner loop gain matrix (composed of proportional $K_{\omega P}$ and $K_{\omega I}$ integral elements)
K_{acc} = Outer loop gain matrix (composed of proportional $K_{acc P}$ and $K_{acc I}$ integral elements)
α = Angle of attack
β = Sideslip angle

DOI: 10.13009/EUCASS2023-376

x_{cg}, x_p = Center of gravity distance from nose, center of percussion distance from center of gravity
C_X, C_Y, C_Z= Nondimensional aerodynamic force coefficients in x_B, y_B, z_B
C_l, C_m, C_n= Nondimensional aerodynamic moment coefficients around x_B, y_B, z_B
Ma = Mach number

1. Introduction

Due to technological developments, both agility and stability are expected from aerial vehicles in highly nonlinear environments with successful flight missions over large flight envelopes. Since the performance requirements of such systems become more challenging, different design features are added to systems; for instance, thrust vector control (TVC) in addition to aerodynamic control (AC) to increase maneuverability and stability under certain conditions. In addition to the developments in the system design, improvements in the control techniques are required at the same time to make full use of the vehicles. For instance, to increase the flight performance and meanwhile to maintain stability, nonlinear control methods could be preferable for highly maneuverable systems. Among nonlinear control strategies, nonlinear feedback linearization (NFL) is a powerful technique. It allows improving the system's capabilities by shaping the poles and zeros of the closed-loop system in a mapped domain with linear tools. Nonlinear Dynamic Inversion (NDI), which is a subclass of NFL, is used in many applications. Some examples of NDI with AC are already studied in [1], [2], and [3]. A system with only TVC is discussed in [4] concerning this problem via redefining the acceleration according to wind frame to apply the NDI. Also note that, accurate aerodynamic angle information required in [4], which may not be possible to provide.
There are few studies for control in boost phase, where the time-variation of the states are extreme due to the speed change in a short duration, especially involving nonlinear methods. Moreover, there is not an NDI study concerning simultaneous TVC and AC in this phase to the knowledge of authors. In this study, NDI autopilots for roll angle and accelerations in the pitch and yaw channels are designed for a system that has AC fins and jet vanes for TVC, which are used simultaneously. The two-loop cascaded autopilot structure is designed, where the inner loop is composed of the angular rate dynamics, which is faster than the outer loop, the acceleration loop. The Proportional-Integral (PI) controllers with second-order reference models are preferred to increase the stability under uncertainties and disturbances. A physically inspired output redefinition at the center of percussion is adapted from [5] to overcome the non-minimum phase characteristic of the system and guarantee internal dynamics stability. The autopilot performances are demonstrated with a high-fidelity mathematical model, and it is compared with ad-hoc scheduled linear autopilots designed as given in [6]. Moreover, a stability analysis is carried out in the presence of high level of uncertainties. Under such uncertainties and a highly coupled set of commands, the autopilot preserves stability and tracks the reference commands successfully. Moreover, a guided scenario is analyzed via implementing the inertial measurement model including the sensor uncertainties, and with the lack of information such as angle of attack and side slip. Even in such challenging conditions, the performance of the autopilot is satisfactory. Thus, this study presents promising results for such an agile system, which has both TVC and AC in the boost phase, while filling the gap in the literature.

2. Mathematical Model

2.1 Plant Model

Before designing the autopilot, general equations of motion are described for the plant in this section. An air defense missile is considered here which has various moving controlling parts: four aerodynamic control (AC) fins and four jet vanes for thrust vector control (TVC) both are in cross-configuration. In this study effective aerodynamic elevator (δ_{A_e}), rudder (δ_{A_r}), aileron (δ_{A_e}) and effective thrust jet vane elevator (δ_{T_e}), rudder (δ_{T_r}), aileron (δ_{T_a}) deflections are used as input to the system as outputs of the autopilot.

DOI: 10.13009/EUCASS2023-376

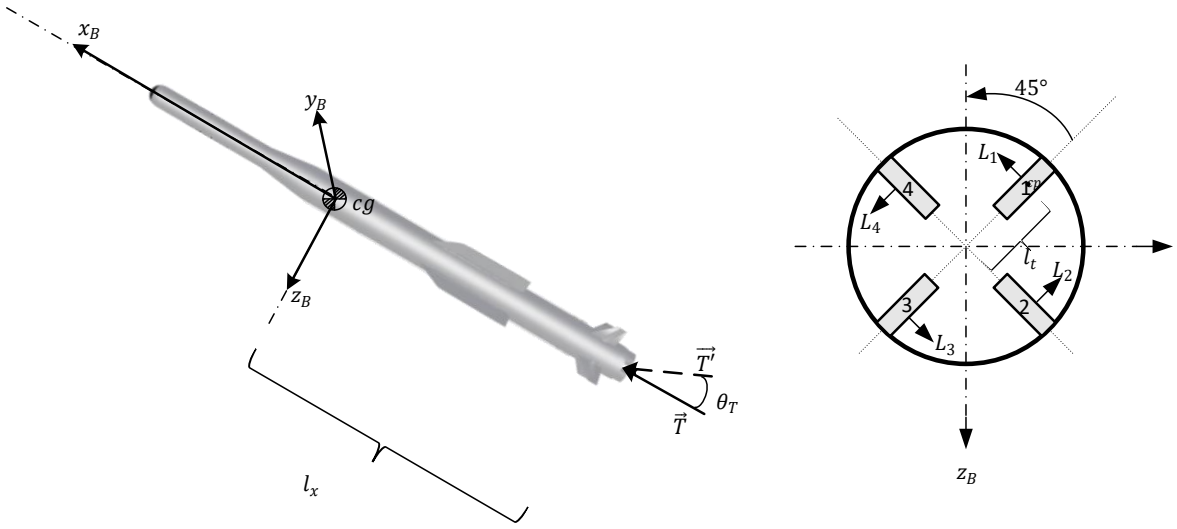

Figure 1: Vehicle Body Axis on the Left and Jet Vanes Illustration on the Right

The translational and rotational motion of the body in a six-degree-of-freedom (6 DoF) environment are described as in Eq. (1) and (2). Eq. (3) and (4) includes mathematical definitions of variables used in previous equations. The 6 DoF modeling here is obtained in light of the [8], also the TVC model is adapted from [9].

$$F_B^{(b)} = \underbrace{\begin{bmatrix} QC_X S_{ref} + T\cos\theta_T \cos\psi_T \\ QC_Y S_{ref} + T\sin\psi_T \\ QC_Z S_{ref} - T\sin\theta_T \cos\psi_T \end{bmatrix}}_{[X \quad Y \quad Z]^T} + L_{BE}\begin{bmatrix} 0 \\ 0 \\ mg \end{bmatrix} = \begin{bmatrix} \dot{u} \\ \dot{v} \\ \dot{w} \end{bmatrix} + \begin{bmatrix} p \\ q \\ r \end{bmatrix} \times \begin{bmatrix} u \\ v \\ w \end{bmatrix} \tag{1}$$

$$M_B^{(b)} = \underbrace{\begin{bmatrix} QC_l S_{ref} l_{ref} - Tl_y \sin\theta_T \cos\psi_T - Tl_z \sin\psi_T \\ QC_m S_{ref} l_{ref} + Tl_z \cos\theta_T \cos\psi_T + Tl_x \sin\theta_T \cos\psi_T \\ QC_n S_{ref} l_{ref} - Tl_y \cos\theta_T \cos\psi_T + Tl_x \sin\psi_T \end{bmatrix}}_{[L \quad M \quad N]^T} = I\begin{bmatrix} \dot{p} \\ \dot{q} \\ \dot{r} \end{bmatrix} + \left(\begin{bmatrix} p \\ q \\ r \end{bmatrix} \times I \begin{bmatrix} p \\ q \\ r \end{bmatrix} \right) \tag{2}$$

$$L_{BE} = \begin{bmatrix} \cos\theta\cos\psi & \cos\theta\sin\psi & -\sin\theta \\ \sin\phi\sin\theta\cos\psi - \cos\phi\sin\psi & \sin\phi\sin\theta\sin\psi + \cos\phi\cos\psi & \sin\phi\cos\theta \\ \cos\phi\sin\theta\cos\psi + \sin\phi\sin\psi & \cos\phi\sin\theta\sin\psi - \sin\phi\cos\psi & \cos\phi\cos\theta \end{bmatrix} \tag{3}$$

$$\vec{l} = \begin{bmatrix} l_x \\ l_y \\ l_z \end{bmatrix}, \; I = \begin{bmatrix} I_{xx} & -I_{xy} & -I_{zx} \\ -I_{xy} & I_{yy} & -I_{yz} \\ -I_{zx} & -I_{yz} & I_{zz} \end{bmatrix} \tag{4}$$

In the above equations, C_X, C_Y, C_Z are non-dimensional force coefficients in x_B, y_B, z_B directions and C_l, C_m, C_n are non-dimensional moment coefficients in roll, pitch, yaw axis. These parameters, depend on the flight conditions as well as aerodynamic angles of missile and aerodynamic fin deflections. Also, non-dimensional parameters have both static and dynamic parts latter depend on angular rates of the body. T is thrust force, θ_T and ψ_T stands for the deflection angle of the thrust from the centerline of the body in longitudinal and lateral axis respectively and both are functions of δ_T which is defined as deflections of jet vanes. L_{BE} is coordinate transformation matrix from body to Earth fixed frame which is a mathematical relation of Euler roll (ϕ), pitch (θ), yaw (ψ) angles. In this study, Earth fixed frame is used interchangeably with the inertial frame since nonrotating flat earth assumption is made. Translational velocities on x_B, y_B, z_B are shown with u, v, w and angular velocities around this respective axis are p, q, r. The moment arm of jet vane forces from the center of gravity (cg) is defined as $\vec{l}$ and its component along x_B is shown as l_x in the Figure 1. Remaining variables included in the equations can be summarized as following. I stands for inertia matrix, m for mass, Q for dynamic pressure, $\vec{g}$ for local gravity vector, S_{ref} and l_{ref} are for reference area and length respectively. Figure 1 included to visualize the variables.

DOI: 10.13009/EUCASS2023-376

2.2 Actuator Model

The control algorithm whose details will be given in the following parts gives outputs as $\delta_{A(e,r,a)}$ and $\delta_{T(e,r,a)}$. However, since the plant has four aerodynamic fins as well as four jet vanes in the tail in cross configuration as in described in Figure 1 the delegation of these effective inputs to fins, referred as $\delta_{A(1,\,2,\,3,\,4)}$ and $\delta_{T(1,\,2,\,3,\,4)}$. Distribution to the fins are made equally as one can check [5] for this distribution. The commands are realized by a second-order control actuator system (CAS) model as described in Eq. (5) and corresponding parameters are given in below Table 1.

Table 1: Parameters of Control Actuation System

CAS Parameters	Representation	Value	Unit
Natural frequency	ω_{cas}	*25*	*Hz*
Damping ratio	ζ_{cas}	*0.6*	-
Angle limit	δ_{max}	*30*	°
Angular rate limit	$\dot{\delta}_{max}$	*500*	°/s

$$\frac{\delta}{\delta_{com}} = \frac{\omega_{cas}^2}{s^2 + 2\zeta_{cas}\omega_{cas} + \omega_{cas}^2} \tag{5}$$

2.3 Inertial Measurement Unit Model

The measurements can be obtained via an inertial measurement unit (IMU) which consists of accelerometer and gyro. These sensors measure the states with an error, therefore a realistic model of sensors with error models given in Table 2 is implemented in the simulation environment. The specifications of the tactical grade IMU HG1930 of Honeywell Aerospace is utilized for the model using the information given in [10] and [11], also misalignment error is assumed.

Table 2: Parameters for Inertial Measurement Unit

Error Type	Accelerometer Channels			Gyro Channels		
	Units	**Measure**	**Value**	**Units**	**Measure**	**Value**
Bias	*mg*	*1σ*	*5*	*°/h*	*1σ*	*20*
Bias in run stability	*mg*	*1σ*	*0.3*	*°/h*	*1σ*	*1*
Scale Factor	*ppm*	*1σ*	*300*	*ppm*	*1σ*	*300*
Random Walk	$fps/\sqrt{h}$	*max*	*0.3*	$°/\sqrt{h}$	*max*	*0.125*
Misalignment	*mrad*	-	*1*	*mrad*	-	*1*

3. Autopilot Design

As it mentioned previously, the study applies an NDI autopilot for the plant considered. NDI linearizes the nonlinear feedback and imposes linear control tools to get the desired output from the system. The idea to linearize the nonlinear feedback is to map the system using a virtual control input. As an example, a nonlinear single input single output system in Eq. (6) is taken and a virtual control input v is selected with linearizing mapping $z(x)$.

$$\dot{x} = f(x) + g(x)u \tag{6}$$

$$z(x) = v \tag{7}$$

After v in Eq. (7) is designed, the input to the real system may be found with Eq. (8).

$$u = g^{-1}(v - f) \tag{8}$$

The idea of NDI is adapted to the acceleration control of a missile here based on [12] and [13]. It is emphasized in [12] that the internal stability of the system should be guaranteed while applying this method. Although its ease to apply, this necessity brings a drawback of the NDI method for the aerodynamic tail-controlled missiles due to plant's

DOI: 10.13009/EUCASS2023-376

nonminimum phase characteristics. To overcome this issue, redefining the outputs according to another point on the missile is considered based on the knowledge that while the transfer function from aerodynamic input to acceleration at the *cg* has zeros on the right half-plane, the transfer function from aerodynamic input to acceleration at the location of IMU is usually is not a non-minimum phase. The physical reason behind this is explained and generalized with the idea of the center of percussion (*cop*) point of the missile in [5]. The *cop* is defined in [14] as a point that forward translational and backward rotational velocity becomes equal in magnitude and opposite in direction. By redefining the acceleration outputs at the *cop* the non-minimum phase issue is handled in this study as in [1]. Then the autopilot is designed with a two-loop cascaded structure such that the inner loop controls the faster states (angular velocities) and the outer loop controls the roll angle and accelerations in pitch and yaw channels.

3.1 Inner Loop Design

Angular velocities in 6-DoF is controlled in the inner loop of the autopilot using NDI. To control angular velocities, using Eq. (2) the inner loop equation is generated to create a loop and control the states as described through Eqs (6-8). Therefore, inner loop dynamics is written in the form of Eq. (9) and the included variables are given in Eqs. (10-12) with previously given definitions of parameters.

$$\begin{bmatrix}\dot{p}\\ \dot{q}\\ \dot{r}\end{bmatrix} = A_{i_{aero}} C_{M_A}(\delta_A) + b_{i_{aero}} + A_{i_{tvc}} C_{M_T}(\delta_T) + b_{i_{tvc}} \tag{9}$$

$$C_{M_A} = \begin{bmatrix} C_{l_\delta}(\delta_A)\\ C_{m_\delta}(\delta_A)\\ C_{n_\delta}(\delta_A)\end{bmatrix},\ C_{M_T} = \begin{bmatrix} \cos\theta_T(\delta_T)\cos\psi_T(\delta_T)\\ \sin\psi_T(\delta_T)\\ -\sin\theta_T(\delta_T)\cos\psi_T(\delta_T)\end{bmatrix} \tag{10}$$

$$A_{i_{aero}} = QS_{ref}l_{ref}\begin{bmatrix} 1/I_{xx} & 0 & 0\\ 0 & 1/I_{yy} & 0\\ 0 & 0 & 1/I_{zz}\end{bmatrix},\ b_{i_{aero}} = \begin{bmatrix} \frac{L + I_{zx}\dot{r} - qr(I_{zz} - I_{yy}) + I_{zx}pq}{I_{xx}}\\ \frac{M - rp(I_{xx} - I_{zz}) - I_{zx}(p^2 - r^2)}{I_{yy}}\\ \frac{N + I_{zx}\dot{p} - pq(I_{yy} - I_{xx}) - I_{zx}qr}{I_{zz}}\end{bmatrix} \tag{11}$$

$$A_{i_{tvc}} = T\begin{bmatrix} 0 & -l_z & l_y\\ l_z & 0 & -l_x\\ -l_y & l_x & 0\end{bmatrix},\ b_{i_{tvc}} = \begin{bmatrix}0\\0\\0\end{bmatrix} \tag{12}$$

Virtual control input for the inner loop is selected as in Eq. (13) where $\omega=[p\ q\ r]^T$. To design the controller a second-order reference model is utilized in every channel with damping ratio ζ_{rm} and corresponding natural frequency ω_{rm_ω}. PI controller is introduced and the gain matrix K_ω is composed of proportional and integral gains of three channels each can be found as in Eq. (14) by assuming perfect inversion process. More detail on PI controller design for NDI controllers are given in [15].

$$v_i = [\dot{p}\quad \dot{q}\quad \dot{r}]^T = K_\omega \begin{bmatrix} \omega_{ref} - \omega\\ \int \omega_{ref} - \omega\end{bmatrix} + \dot{\omega}_{ref} \tag{13}$$

Although, scheduling the gains according to flight conditions are not necessary for NDI autopilots, in simulation, the gains are calculated dynamically by adapting a second order reference model according to the dynamic pressure, i.e., for a faster reference model higher value of reference natural frequency is used under higher dynamic pressures.

$$K_{\omega_P} = 2\zeta_{rm}\omega_{rm_\omega},\ K_{\omega_I} = \omega^2_{rm_\omega} \tag{14}$$

After designing the virtual control inputs given in Eq. (13) and inserting them into the Eq. (9) the inputs to the system δ_A and δ_T should be drawn from Eq. (9). This problem might have multiple solutions because of one equation and two unknowns which brings control allocation need in the boost phase between AC and TVC. This allocation is a whole another subject and analyzed in another study of authors in [16] while this study focuses on the general NDI autopilot solution for the given system. Briefly for this study, this problem is overcome by allocating the total desired moment

DOI: 10.13009/EUCASS2023-376

between the AC and TVC parts of Eq. (9). This allocation is done dynamically in the simulation in line with the effectiveness of each control type. This effectiveness, described as E in the Figure 2, is defined as the ratio of the moment produced by TVC per unit δ_T , to the moment produced by AC per unit δ_A.

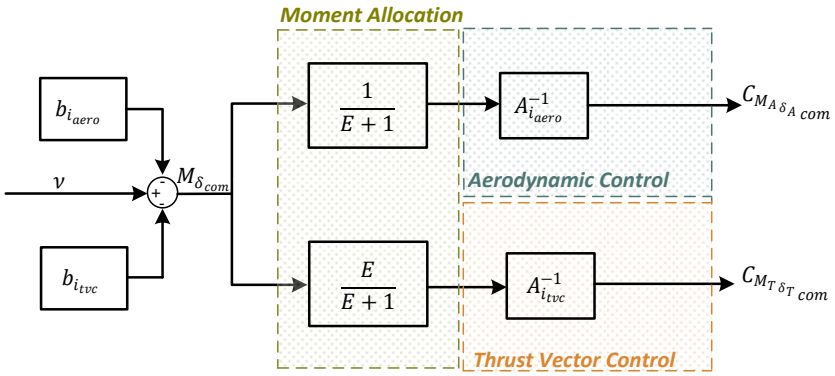

Figure 2: Control Allocation Scheme

3.2 Outer Loop Design

The outer loop aims to control the roll angle with lateral and longitudinal accelerations. To do that, this loop takes the commands for control variables and produces angular velocity commands to be realized by the inner loop. As mentioned before, the outputs as well as the control variables of the problem shown with vector ($\vec{y}$) is redefined according to the *cop* point which is along the x_B axis of the missile and at a distance x_p from the *cg*. Afterward, lateral (a_{p_y}) and longitudinal (a_{p_z}) accelerations at *cop* is calculated in Eq. (15).

$$\vec{y} = \begin{bmatrix} \phi \\ a_{p_y} \\ a_{p_z} \end{bmatrix} = \begin{bmatrix} \int (p + (q\sin\phi + r\cos\phi)\tan\theta)dt \\ (QC_Y S_{ref} + T\sin\psi_T)/m + x_P(\dot{r} + pq) \\ (QC_Z S_{ref} - T\sin\theta_T\cos\psi_T)/m + x_P(-\dot{q} + pr) \end{bmatrix} \quad \textbf{(15)}$$

Again, similar strategy with the inner loop followed to apply NDI method for the outer loop. Eq. (15) can be brought to the form of Eq. (16) which is compatible with Eq. (6) and NDI can be applied such that this outer loop produces commands to the inner loop. One may obtain the outer loop matrices A_o and b_o by taking the derivative of Eq. (15) and for more details may refer to [5].

$$\dot{y} = f(p, q, r) = A_o \begin{bmatrix} p \\ q \\ r \end{bmatrix} + b_o \quad \textbf{(16)}$$

The virtual control inputs for outer loop selected as $\nu_o = \dot{y}$ and designed similar to the inner loop. Second order reference models and PI controllers are used which result in the control structure in Eq. (17).

$$[p_{com} \quad q_{com} \quad r_{com}]^T = A_o^{-1}\left(- b_o + K_{acc} \begin{bmatrix} y_{ref} - y \\ \int y_{ref} - y \end{bmatrix} + \dot{y}_{ref} \right) \quad \textbf{(17)}$$

The gain matrix K_{acc} includes proportional and integral gains for three channels those are calculated similar to Eq. (14) which are again calculated by changing the reference model dynamically in simulation. In order to visualize and summarize the procedure given above clear, an illustration of the acceleration autopilots is given in Figure 3.

DOI: 10.13009/EUCASS2023-376

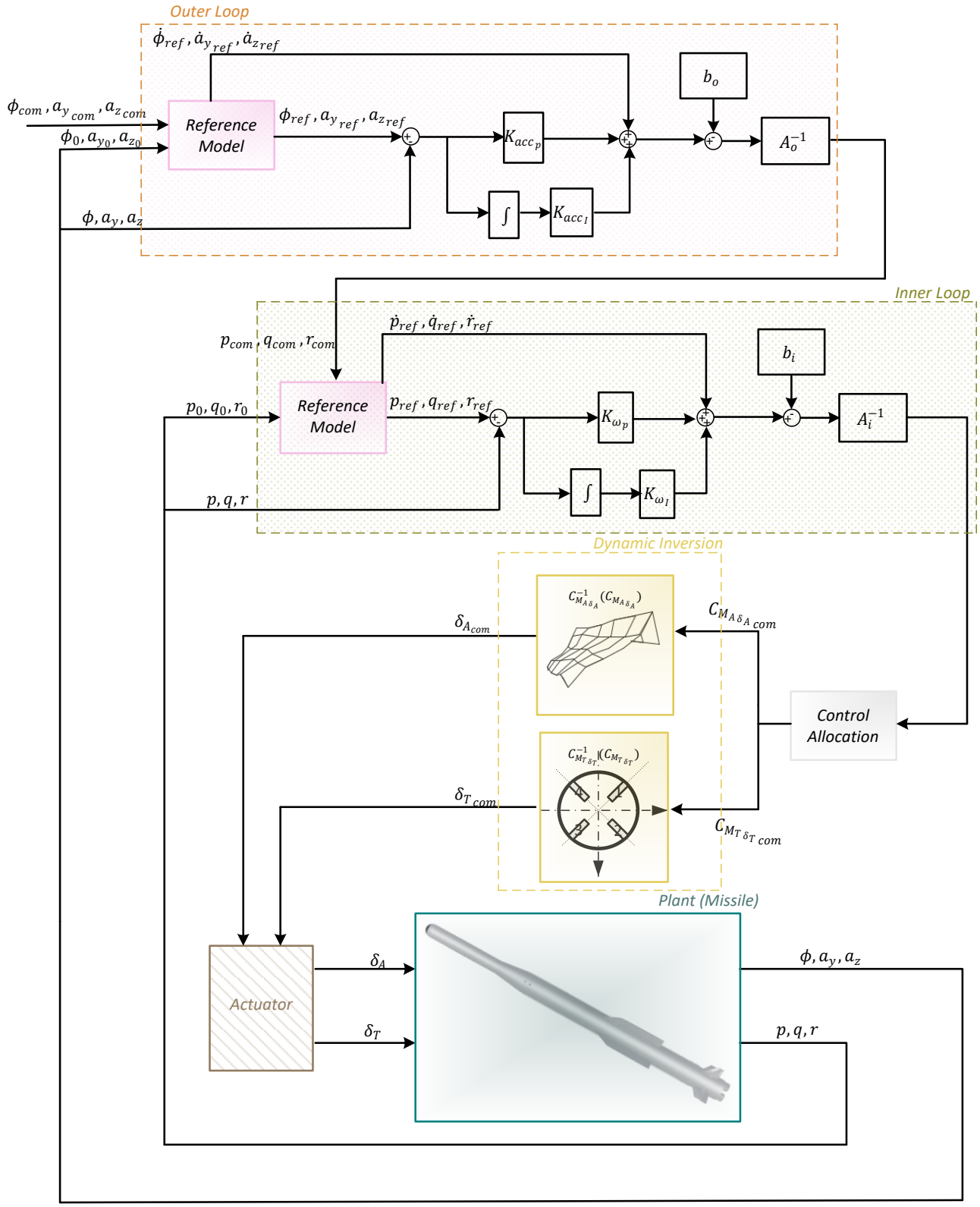

Figure 3: Nonlinear Dynamic Inversion Autopilot Scheme

DOI: 10.13009/EUCASS2023-376

4. Simulation Results

In this section three set of simulation results are tabulated. The results are obtained including both boost and coast phase of the flight. The first one is the nominal results that consist of the results for the designed system with all the necessary inputs for the autopilot provided; such that flight parameters, angular rates, angles and accelerations are assumed as measured perfectly with actuator model implemented as in described in section 2.2. Second, under four sets of uncertainties the system is tested if it is still capable to control the system. Last, the autopilot is run in a guided scenario with realistic measurements modeled with IMU. Moreover, for the last scenario, the measurements that are usually not easy to measure or observe such as aerodynamic angles are taken zero ($\alpha = 0, \beta = 0$) and angular velocity rates ($\dot{p}, \dot{q}, \dot{r}$) are obtained utilizing a filter model to get the corresponding derivatives . All the results are given in a normalized form due to confidentiality issues and the value used for normalization is displayed in the corresponding figure labels.

4.1 Nominal Results

As the test scenario, a challenging command set is generated that results in a highly coupled dynamics. First, results of the autopilot is shown in Figure 4 in order to observe the behavior of the autopilot closely. Acceleration tracking performance at the *cg* and at the center of percussion point *p* of the missile is as expected. The nonminimum phase behavior of the system can be also observed in the accelerations with respect to *cg*. Later, the results in all three channels are compared with a baseline autopilot which is designed with neglecting the coupling terms and using linear control theory as described in [6]. In Figure 5 and Figure 6 it is seen that baseline autopilot is not able to track the command for the nominal case. That is expected due to its lack of information about the bank-to-turn movement. Whereas NDI autopilots track the reference signals under highly varying speed, although the commands are challenging. Noticing that the deviations from the reference signal occurs at the beginning of the flight where the speed is low.

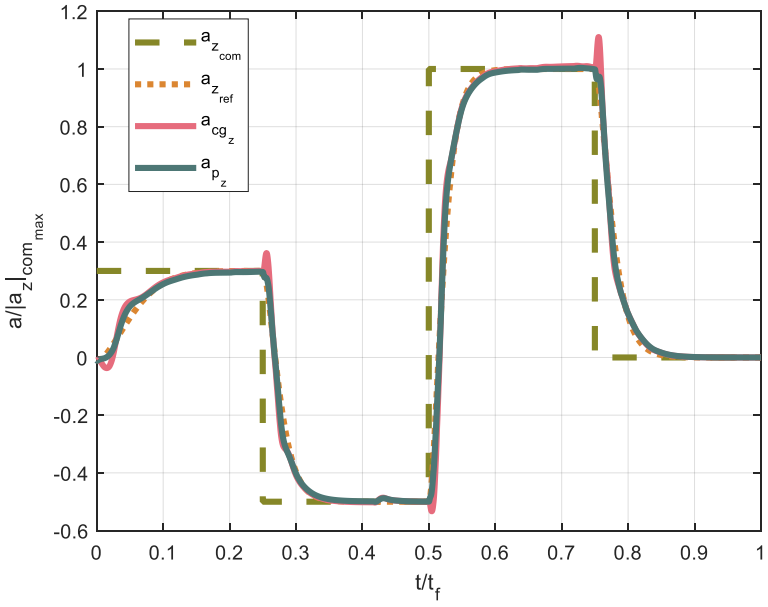

Figure 4: Nominal Results for Pitch Channel with NDI

DOI: 10.13009/EUCASS2023-376

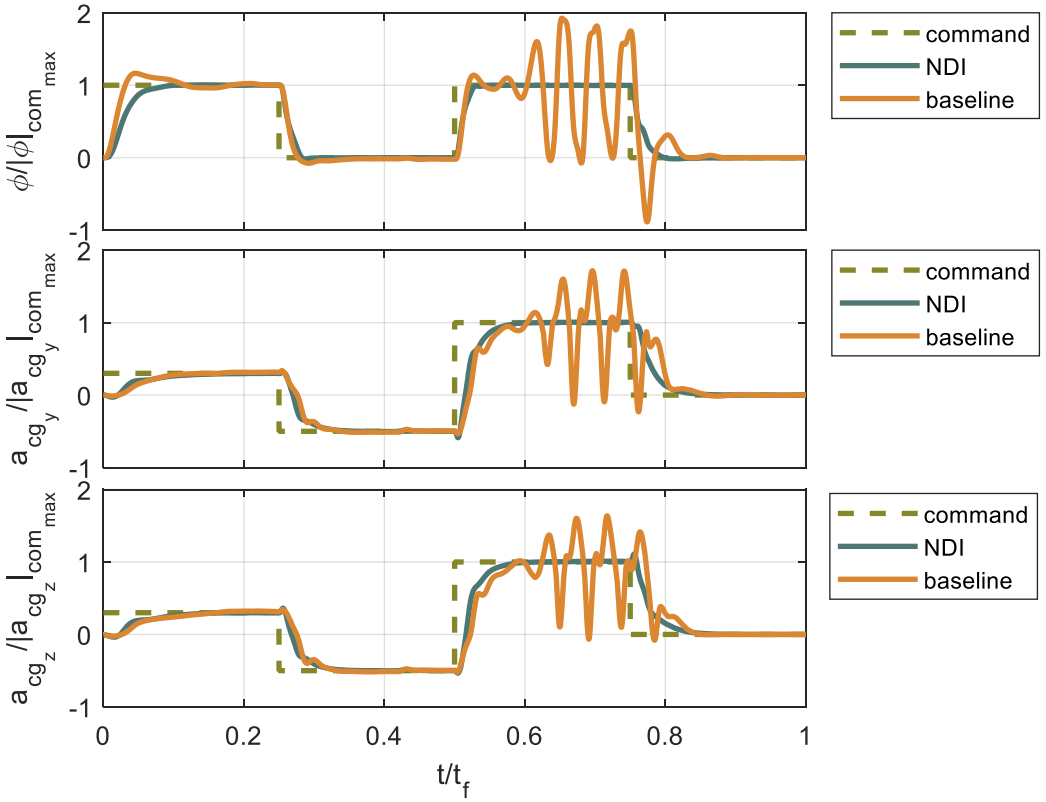

Figure 5: Nominal NDI Results Compared with a Baseline Autopilot

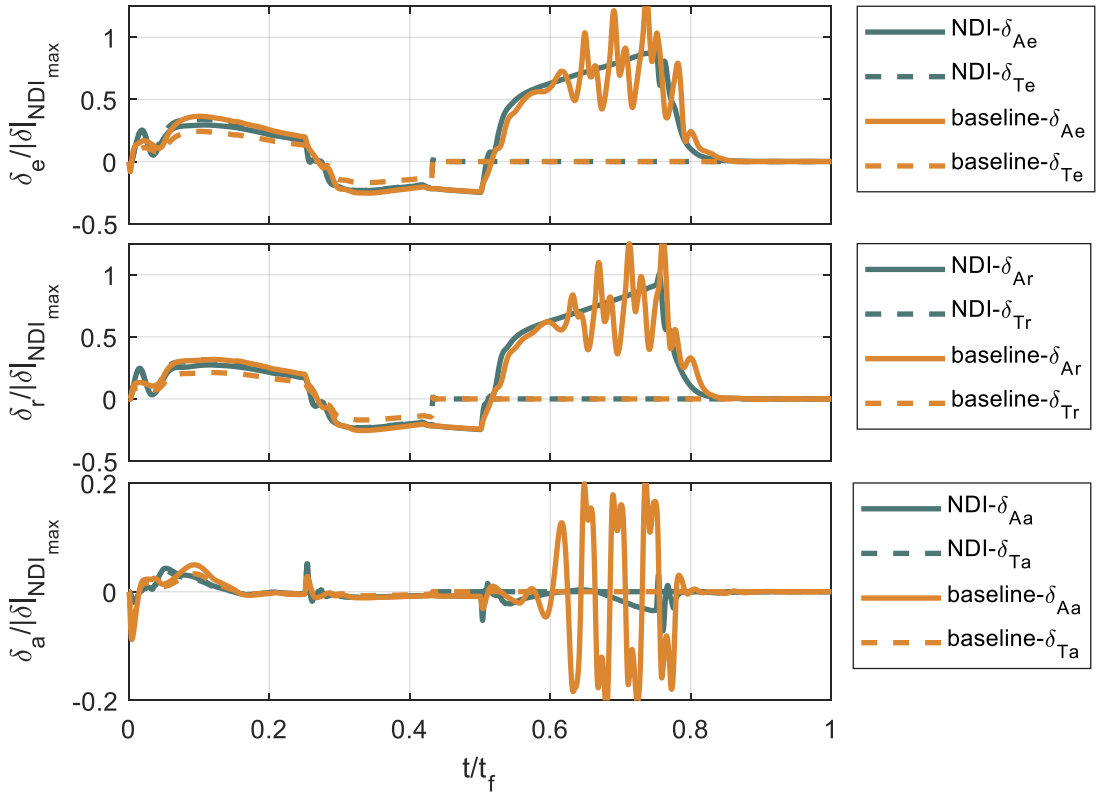

Figure 6: Nominal NDI Deflections Compared with a Baseline Autopilot

DOI: 10.13009/EUCASS2023-376

4.2 Sensitivity Analysis

In this section four uncertainty case is generated as shown in Table 3. All the uncertainties are given as percentages to the corresponding parameters. The uncertainties are modeled in the Simulink as follows. The (+) sign in Table 3 represents that the corresponding value is higher in real part of the simulation or equivalently the controller knows the value less than it is with the given percentage. The (-) sign represents vice versa.

Table 3: Uncertainties

Variable	Symbol	Uncertainty (%)	Case -1	Case-2	Case-3	Case-4
Mass	m	*1*	+	+	+	-
Inertia	I	*5*	+	+	-	-
Center of Gravity	x_{cg}	*3*	+	-	-	-
Non-dimensional Force Coefficients	C_X, C_Y, C_Z	*25*	+,+,+	-,-,-	+,+,+	-,-,-
Non-dimensional Dynamic Force Coefficients	C_{X_d}, C_{Y_d}, C_{Z_d}	*25*	+,+,+	-,-,-	+,+,+	-,-,-
Non-dimensional Moment Coefficients	C_l, C_m, C_n	*25*	+,+,+	-,-,-	+,+,+	-,-,-
Non-dimensional Dynamic Moment Coefficients	C_{l_d}, C_{m_d}, C_{n_d}	*25*	+,+,+	-,-,-	+,+,+	-,-,-
Thrust Force	T	*10*	+	+	-	+
Thrust Deflection Angles	θ_T, ψ_T	*5*	+,+	-,-	-,-	+,+
Aerodynamic Angles	α, β	*10*	+,+	-,-	+,-	-,+
Dynamic Pressure	Q	*5*	+	+	-	-
Mach Number	Ma	*5*	+	-	+	-

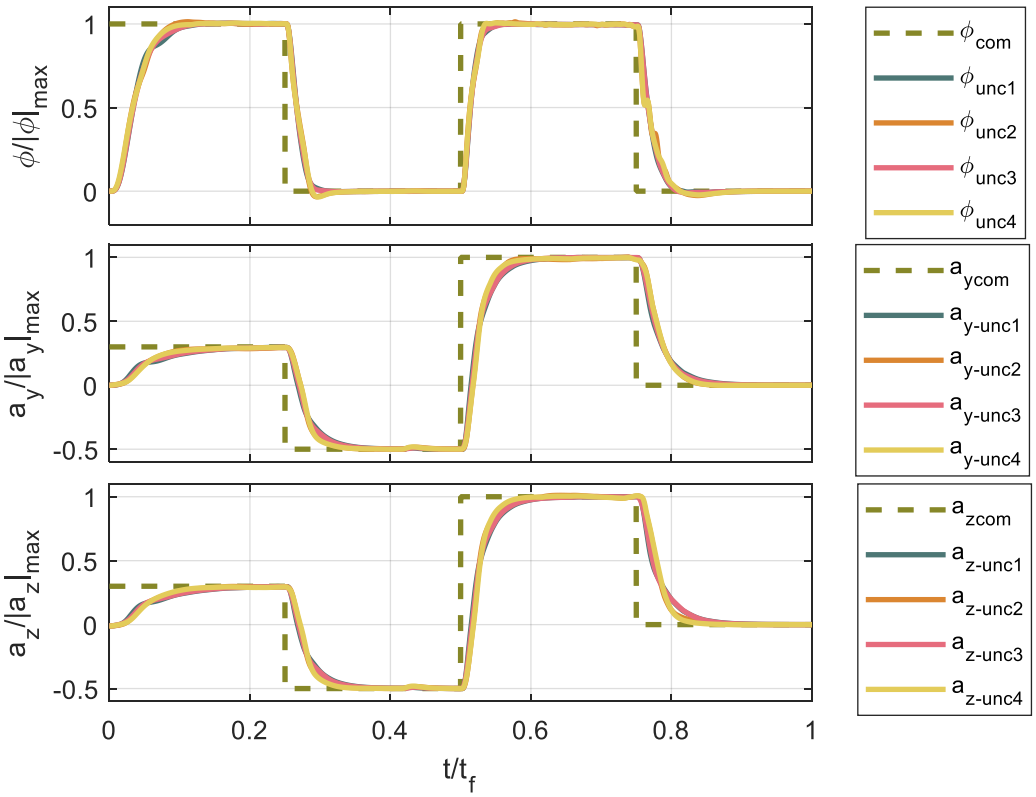

Figure 7: Outputs with Uncertainties

DOI: 10.13009/EUCASS2023-376

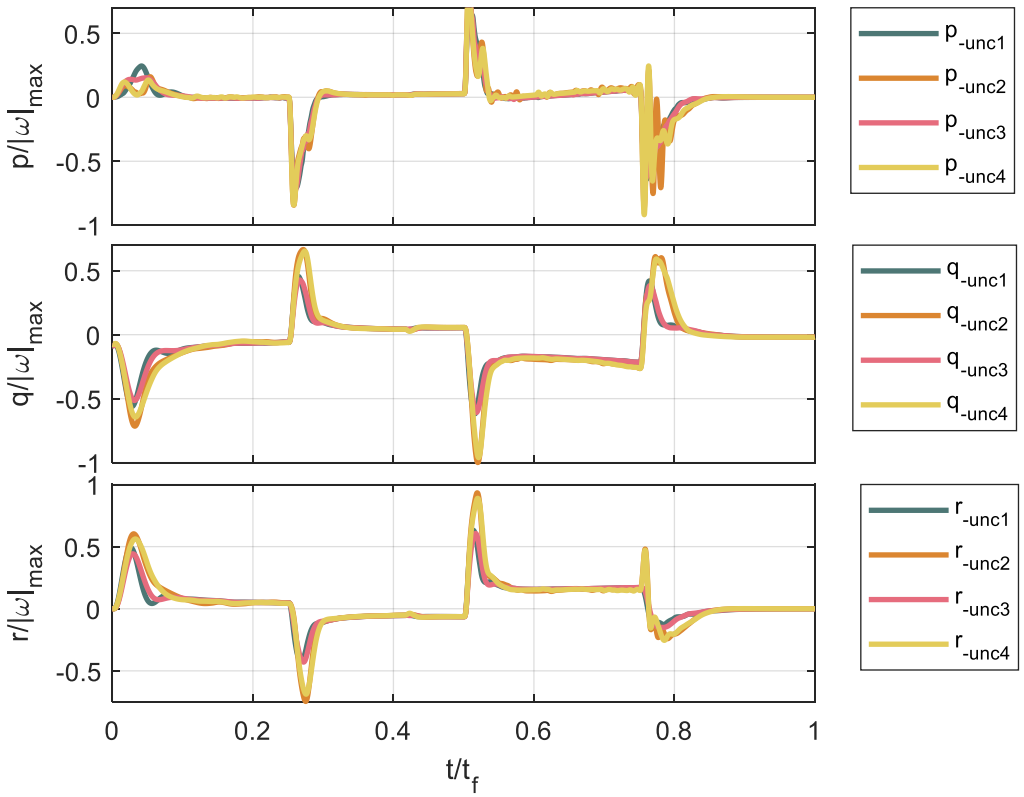

Figure 8: Angular Velocities with Uncertainties

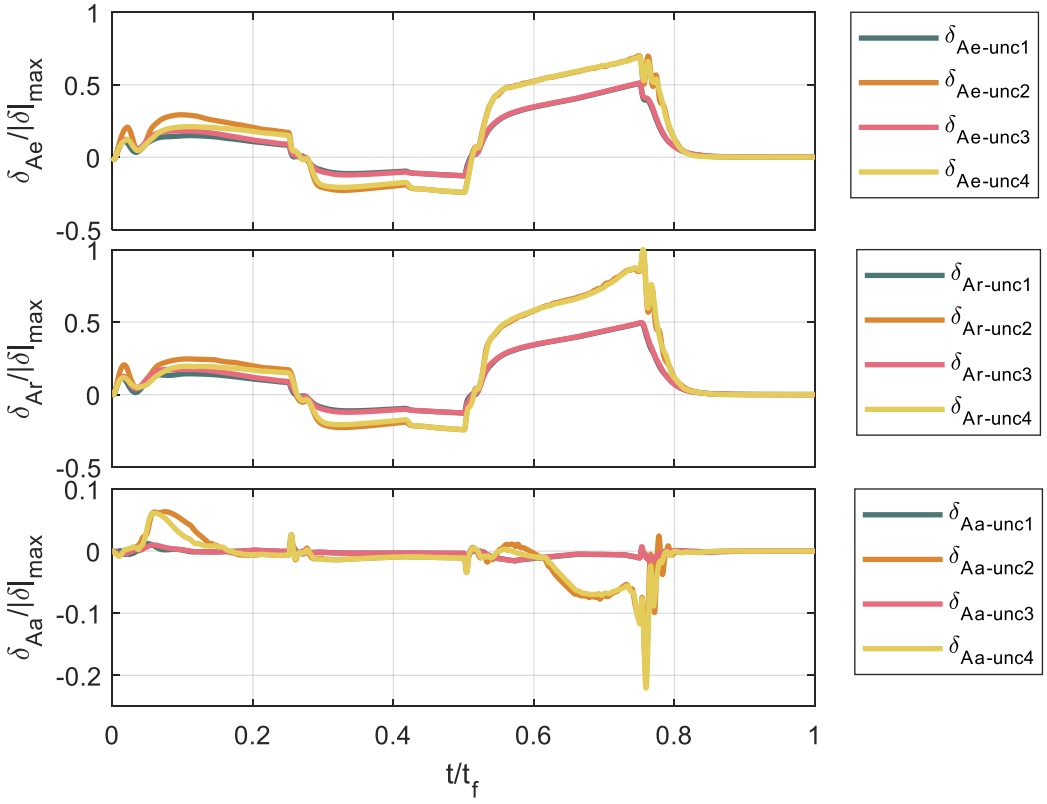

Figure 9: Effective AC Fin Deflections with Uncertainties

DOI: 10.13009/EUCASS2023-376

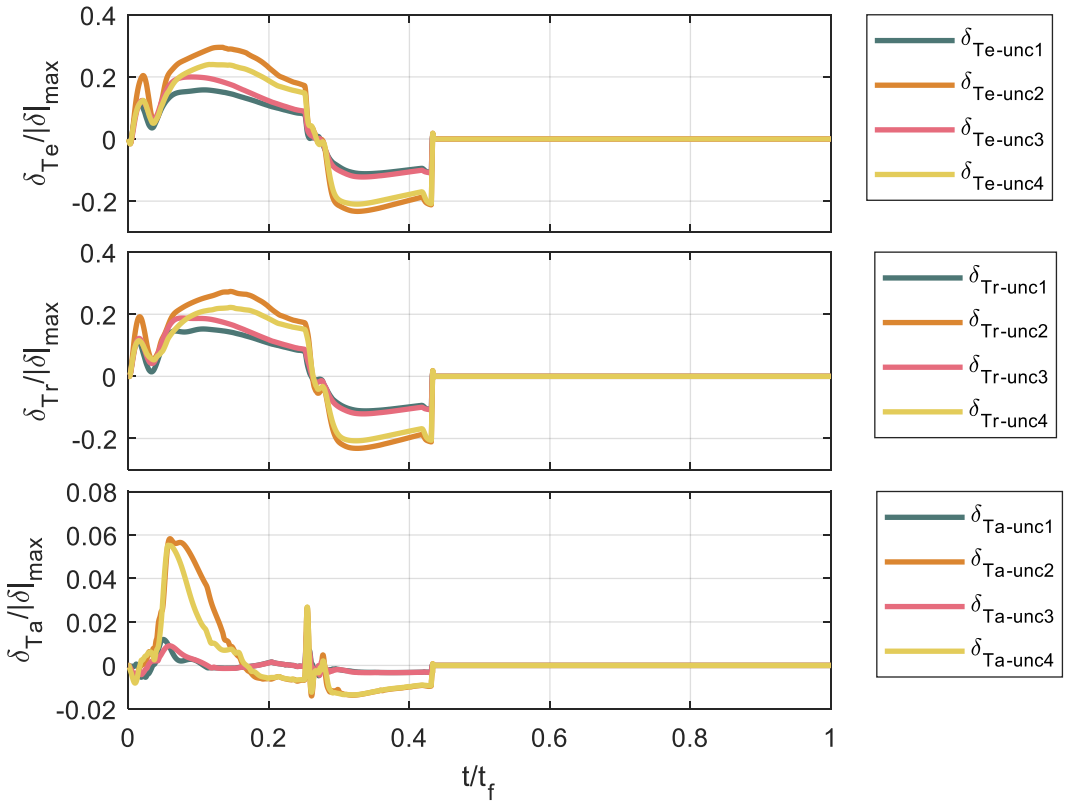

Figure 10: Effective TVC Jet Vane Deflections with Uncertainties

In Figure 7 the autopilot tracking performance is shown for the different uncertainties. Although some degradation in the tracking performance is seen, the stability within these cases is preserved. There are some fluctuations in the corresponding angular velocities as displayed in Figure 8. Effective aerodynamic fin deflections in Figure 9 and effective TVC jet vane deflections in Figure 10 differed for each case considerably due to the uncertainties. Note that jet vane deflections are only available for the boost phase. In most studies, NDI autopilots are criticized about its challenges to use in real life applications due to the requirements of accurate measurements of parameters. This analysis shows that autopilot may not require knowledge of aerodynamic and flight parameters as precise as it is thought and NDI autopilots may preserve robustness under noticeable uncertainties.

4.3 Guided Scenario

Finally, a guided scenario is tested in simulation. For this case, aforementioned IMU model is also included in the analysis. As a guidance strategy Pure Proportional Navigation from [17] is adapted with effective navigation constant, $N' = 5$.

DOI: 10.13009/EUCASS2023-376

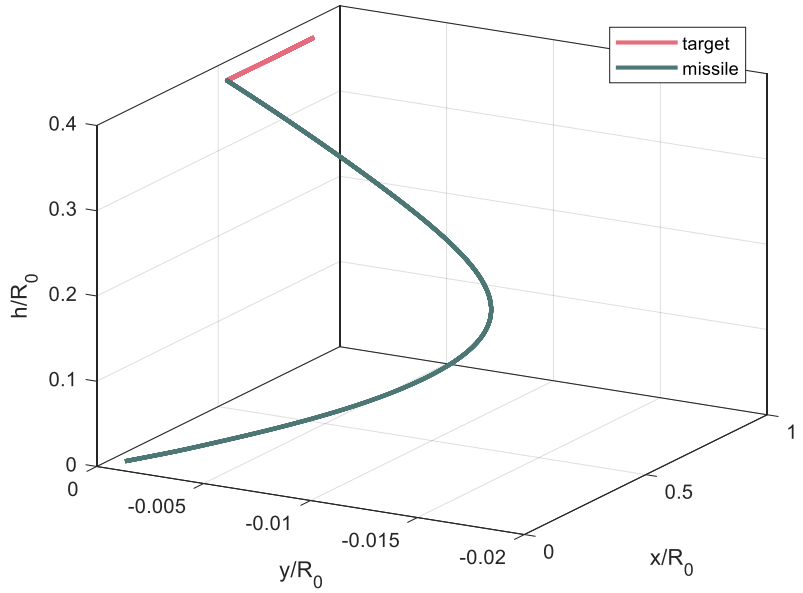

Figure 11: Trajectories of the Guided Scenario

As it is seen from the trajectories in Figure 11, an agile maneuver is required since the target is behind the fire direction of the missile. For this flight the commands from the guidance algorithm and the responses of autopilots can be observed in Figure 12. Autopilots track the command in the presence of measurement errors and noises.

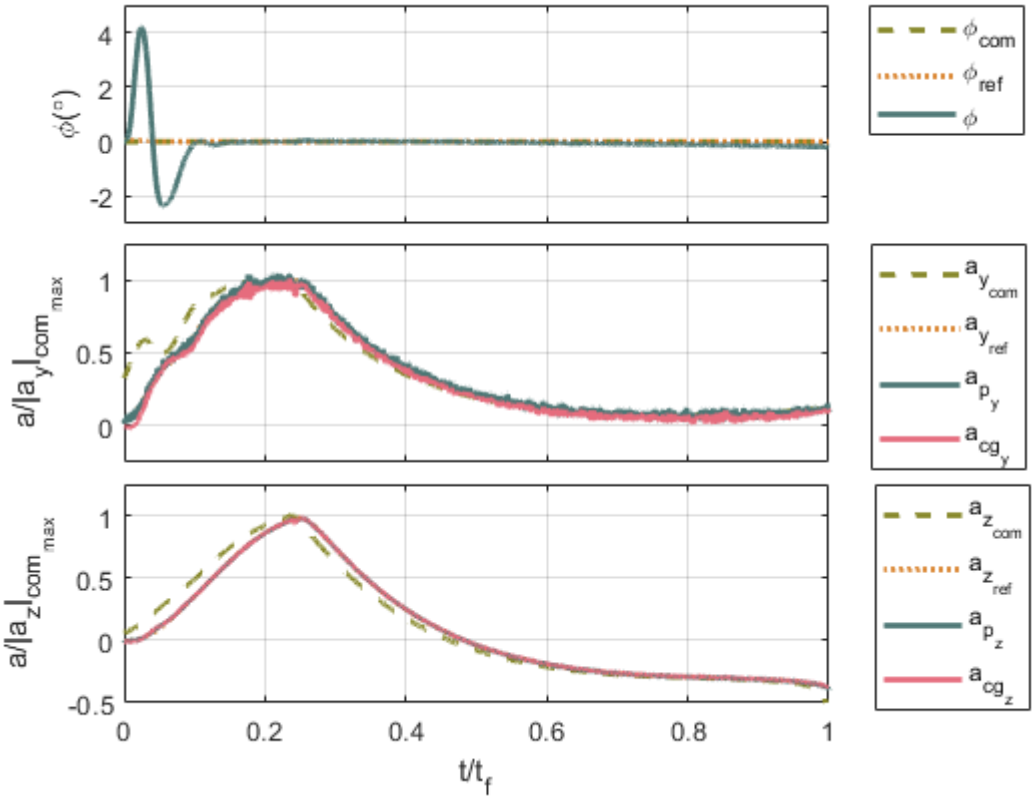

Figure 12: Output Tracking Performance of the Guided Scenario

It is observed that the missile with NDI autopilot is capable of capturing the target within the restricted information of the states, which is valuable for practical purposes.

DOI: 10.13009/EUCASS2023-376

5. Conclusion

In this paper, an NDI autopilot is designed for an air defense missile with aerodynamic and thrust vector control. A two-loop cascaded structure with a second-order reference model and the PI controller is applied within the autopilot structure. The reference model is chosen compatible with the flight conditions such that for higher dynamic pressure, a faster model is utilized. Then, the study is extended the analysis in the presence of the uncertainties, where the autopilot preserves the stability within the uncertainties for a highly coupled set of commands and tracks the commands with acceptable deviations. After the sensitivity analysis, a guided scenario is examined with implementing an IMU model and without the information of aerodynamic angles. In such a case, the missile hits the target by following the commands of the guidance algorithm. This study presents promising results on NDI such that its application to the systems in a practical sense may be feasible. Further analysis and enhancements will be done as future work to ensure stability and robustness under saturation.

References

[1] Peter, F., Leitão, M., & Holzapfel, F. (2012). Adaptive augmentation of a new baseline control architecture for tail-controlled missiles using a nonlinear reference model. *AIAA Guidance, Navigation, and Control Conference*. https://doi.org/10.2514/6.2012-5037

[2] Tiryaki Kutluay, K., & Yavrucuk, İ. (2010). *Adaptive Control of Guided Missiles* (thesis). Retrieved September 20, 2021, from http://etd.lib.metu.edu.tr/upload/12613083/index.pdf.

[3] Tipán, S., Thai, S., Proff, M., & Theodoulis, S. (2020). Nonlinear dynamic inversion autopilot design for dual-spin guided projectiles. *IFAC-PapersOnLine*, *53*(2), 14827–14832. https://doi.org/10.1016/j.ifacol.2020.12.1926

[4] Lee, C.-H., Jun, B.-E., Shin, H.-S., & Tsourdos, A. (2017). Nonlinear acceleration controller for exo-atmospheric and endo-atmospheric interceptors with TVC. *2017 25th Mediterranean Conference on Control and Automation (MED)*. https://doi.org/10.1109/med.2017.7984110

[5] Peter, F., Holzapfel, F., Baier, H., & Holzapfel, F. (2018). Nonlinear and adaptive missile autopilot design (thesis). Retrieved September 20, 2021, from https://mediatum.ub.tum.de/doc/1416304/1416304.pdf.

[6] Gezer, R. B., & Kutay, A. T. (2014). Robust model following control design for missile roll autopilot. 2014 UKACC International Conference on Control (CONTROL). https://doi.org/10.1109/control.2014.6915107

[7] Buschek, H. (2003). Design and flight test of a robust autopilot for the iris-T air-to-air missile. *Control Engineering Practice*, *11*(5), 551–558. https://doi.org/10.1016/s0967-0661(02)00063-1

[8] Etkin, B. (1972). Reference Frames and Transformations, General Equations of Unsteady Motion. In *Dynamics of Atmospheric Flight* (pp. 104–189). essay, John Wiley & Sons , Inc.

[9] Tekin, R., Atesoglu, Ö., & Leblebicioglu, K. (2010). Modeling and vertical launch analysis of an aero- and thrust vector controlled surface to air missile. *AIAA Atmospheric Flight Mechanics Conference*. https://doi.org/10.2514/6.2010-7639

[10] *HG1930 inertial measurement unit*. Aerospace. (n.d.). Retrieved December 27, 2021, from Tekin, R., Atesoglu, Ö., & Leblebicioglu, K. (2010). Modeling and vertical launch analysis of an aero- and thrust vector controlled surface to air missile. *AIAA Atmospheric Flight Mechanics Conference*. https://doi.org/10.2514/6.2010-7639

[11] *Keyword Analysis & Research: HG1930*. free tracking. (n.d.). Retrieved December 27, 2021, from https://www.eigolink.net/find/hg1930

[12] Slotine, J.-J. E., & Li, W. (1991). Part 2 : Nonlinear Control Systems Design. In *Applied Nonlinear Control: An introduction* (pp. 191–392). essay, Prentice-Hall.

[13] Khalil, H. K. (2002). 13 Feedback Linearization. In *Nonlinear systems* (pp. 505–551). essay, Prentice Hall.

DOI: 10.13009/EUCASS2023-376

[14] Center of Percussion. (n.d.). Retrieved December 28, 2021, from https://sciencedemonstrations.fas.harvard.edu/presentations/center-percussion

[15] Zhang, F., & Holzapfel, F. (2015). Flight control using physical dynamic inversion. *AIAA Guidance, Navigation, and Control Conference*. https://doi.org/10.2514/6.2015-1758

[16] Bıyıklı, R.,Tekin, R., & Yavrucuk, I. (2022). Control allocation strategies for a hybrid controlled missile with NDI autopilot. *13th Asian Control Conference (ASCC)*, Jeju, Korea, doi: 10.23919/ASCC56756.2022.9828187.

[17] Tekin, R., & Erer, K. S. (2015). Considerations on boost phase modeling and guidance command generation. *AIAA Guidance, Navigation, and Control Conference*. https://doi.org/10.2514/6.2015-0862